Research Article Vol. 30, No. 11 / 23 May 2022 / Optics Express 19030
Optics EXPRESS

# Highly-sensitive sensor based on toroidal dipole governed by bound state in the continuum in dielectric non-coaxial core-shell cylinder

YANYAN HUO,[1,2,3] XIN ZHANG,[1,2] MENG YAN,[1,2] KE SUN,[1,2] SHOUZHEN JIANG,[1,2] TINGYIN NING,[1,2] AND LINA ZHAO[1,2,4]

[1]Shandong Provincial Key Laboratory of Optics and Photonic Device & Shandong Provincial Engineering and Technical Center of Light Manipulations, School of Physics and Electronics, Shandong Normal University, Jinan 250358, China
[2]Collaborative Innovation Center of Light Manipulations and Applications, Shandong Normal University, Jinan 250358, China
[3]yanyanhuo2014@sdnu.edu.cn
[4]lnzhao@sdnu.edu.cn

**Abstract:** The electromagnetic fields distributed on the surface region of the nanostructure is very important to improve the performance of the sensor. Here, we proposed a highly sensitive sensor based on toroidal dipole (TD) governed by bound state in the continuum (BIC) in all-dielectric metasurface consisting of single non-coaxial core-shell cylinder nanostructure array. The excitation of TD resonance in a single nanostructure is still challenging. The designed nanostructure not only supports TD resonance in a single nanostructure but also has very high *Q*-factor. More importantly, its electric field distributes at the surface of outer cylinder-shell, which is very suitable for biosensing. To evaluate the sensing performance of our proposed structure, we investigated the sensitivity and the figure of merit (*FOM*) of nanostructure with different structural parameters. Maximum sensitivity and *FOM* can reach up to 342 nm/RIU and 1295 when the asymmetric parameter $d$ =10 nm. These results are of great significance to the research of TD resonance and the development of ultrasensitive sensor.



## 1. Introduction

Sensors based on plasmonic nanostructures exhibit high sensitivity caused by the strong electric fieldat the position of the analyte [1]. Low concentrations of chemical biomolecules or even single molecules can be detected by them [2]. Unfortunately, plasmonic nanostructures have very high losses because of the intrinsic absorption of plasmonic metals [3–5], which represents a lower quality factor (*Q*-factor) and limits the sensing performance. Compared to plasmonic nanostructures, dielectric nanostructures do not suffer from absorption losses. In recent years, high refractive index dielectric nanostructures have attracted extensive attention in the context of metasurfaces and nanoantennas [6–10]. They can control light efficiently and flexibly at the nanoscale [11,12], and open up an opportunity forbiosensing applications [6,13–15]. Some dielectric nanoparticles exhibited high sensitivity up to 300 nm/RIU, which is comparable to localized surface plasmon resonance sensors [6,14]. However, optically resonant sensors are characterized not only by the shift in the resonance wavelength per refractive-index-unit change (*S*) but also by the high *Q*-factor of the resonance mode. The figure of merit (*FOM*) is another characteristic parameter for optically resonant sensors, which is given by $FOM = S \cdot Q/\lambda$, where, $\lambda$ is the wavelength of the resonance mode. When combining the sensitivity (*S*) with the *Q*-factor, *FOM* of these dielectric nanoparticles is relatively low due to the lower *Q*-factor.

Toroidal dipole (TD), as the third fundamental family of electromagnetic multipole, is a circular head-to-tail arrangement of magnetic or electric dipoles and the poloidal currents

#456362 https://doi.org/10.1364/OE.456362
Journal © 2022 Received 16 Feb 2022; revised 23 Apr 2022; accepted 30 Apr 2022; published 16 May 2022

Optics EXPRESS

that flow on a torus along its meridians [16]. However, it is very difficult to be detected in experiments because of the relatively weak coupling to the incident light. They are usually masked by the contribution of the conventional magnetic dipole (MD) or electric dipole (ED). In order to enhance TD response, a variety of metamaterials have been proposed. For example, three-dimensional (3D) nanostructures composed of four split wireloops [17], sun-like aperture [18], bi-material cantilever structures [19], and dumbbell-shaped aperture [20], etc. There are also two-dimensional (2D) nanostructures composed of asymmetry of the clusters structure to enhance TD [21–23]. Although these metamaterials can support TD resonances, they have a very complex shape. Compared of 3D and 2D asymmetric cluster nanostructure, the fabrication of metamaterials composed of single nanostructure is easier. TD is drawing attention to the dielectric metamaterial because of its high $Q$-factor [24,25], which have been used as a platform implementing ultrasensitive sensors [21,25–27].

The true bound state in the continuum (BIC) is a mathematical object with an infinite $Q$-factor and zero resonance line-width [21,28,29]. However, BIC is symmetry-protected and cannot be observed in real systems. It is often in the form of quasi-BIC with finite $Q$-factor and nonzero line-width [30,31]. Quasi-BIC has been widely used in nonlinear optics, nanolasing and so on due to its high $Q$-factor and large electric field enhancement [32–35]. And it is very suitable for biosensing because of high $Q$-factor and narrow line-width [36–40]. However, the resonant mode of the proposed quasi-BIC are mostly Mie-type modes or whispering gallery modes, the field are mainly stored in the high-index material [34]. While for chemical sensors, the chemical biomolecules are usually attached to the surface of the nanostructures. Therefore, nanostructures with the electromagnetic fields stored at the surface region is beneficial to improve the sensing performance, which has been demonstrated in references [39–43].

In this letter, we proposed a sensor based on TD resonance excited by a quasi-BIC in high-index dielectric metasurface composed of non-coaxial core-shell cylinder array. The TD resonance is achieved by symmetry breaking in an individual dielectric nanostructure under plane wave illumination, which can transform BIC to quasi-BIC by controlling the asymmetry of core-shell cylinder. It has very high $Q$-factor. More importantly, its electric field can be localized at the surface of the outer cylinder shell, which is very suitable for optical chemical biosensing. Combining the high $Q$-factor and strong near-field confinement at the surface of nanostructure, we demonstrated the sensor based on our proposed nanostructure has a high sensitivity of 342 nm/RIU and high *FOM* of 1295 when the asymmetry parameter $d = 10$ nm.

## 2. Numerical model

Figure 1(a) shows the dielectric metasurface nanostructure for biosensing. It composes of an array of periodic non-coaxial core-shell cylinder depositing on a silica substrate with the refractive index $n = 1.5$. The geometric parameters of the non-coaxial core-shell cylinder are illustrated in Fig. 1(a). $P_x = P_y = P$ is the lattice constant of the metasurface. The radii of the outer cylinder shell and the inner cylinder core are $R_1$ and $R_2$. The heights of them are $h_1$ and $h_2$. $d$ is the offset of the axis of the inner cylinder shifts from the axis of the outer cylinder shell along $x$-axis, which can control the symmetry of the nanostructure. When $d = 0$, the core-shell cylinder nanostructure is symmetric in $x$-$y$ plane. When $d \neq 0$, it means that the symmetry of the structure along the $x$-axis is broken, which allows the resonant mode to transform from symmetric-protected BIC to quasi-BIC. High refractive index dielectric material can satisfy the resonant conditions [44,45]. In this letter, the material of the outer cylinder shell is chosen as silicon with refractive index of $n$ =3.67. The material of the inner cylinder core is set as silica with refractive index of $n = 1.5$. In the following calculations, the finite element method (Comsol Multiphysics) is used to accurately calculate the spectral characteristics and the biosensing performance. One period is selected as the simulation domain. Bloch-Floquet periodic boundary conditions are imposed to the boundary of the unit cell in $x$- and $y$-directions. The top boundary is set as the port 1 for

Optics EXPRESS

the light incidence, and the bottom boundary is set as port 2. The transmission spectra of the metasurface are simulated under normal incident light with $x$-polarized. In order to study the biosensing performance, the nanostructures are immersed in water ($n = 1.33$) with a depth of 500 nm.

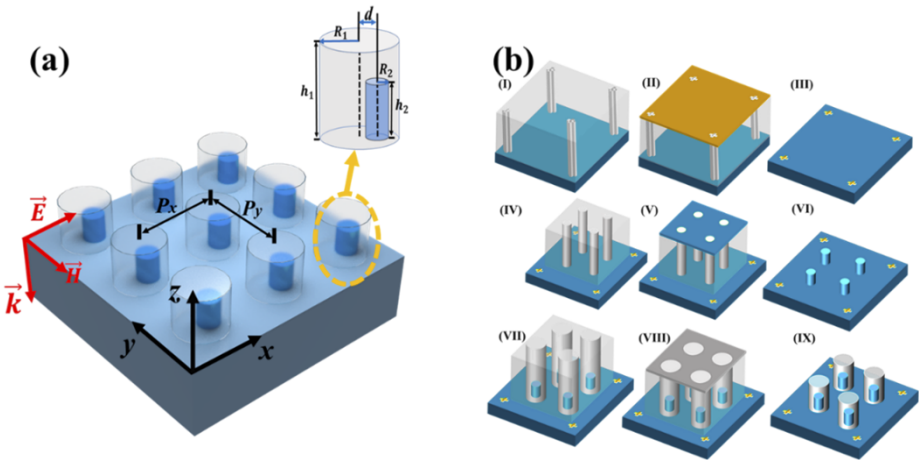


**Fig. 1.** (a) Structure diagram of the periodic non-coaxial core-shell cylinder nanostructure on a silica substrate with period $P_x$=$P_y$= $P$ and the incident light.$\vec{k}$, $\vec{E}$ and $\vec{H}$ are the wavevector, electric field and magnetic field of the incident light, respectively. Inset: The non-coaxial core-shell cylinder with the geometric parameters. $R_1$ and $R_2$ are the radii of the outer cylinder shell and the inner cylinder core. $h_1$ and $h_2$ are the heights of them, respectively. $d$ is the offset of the inner cylinder axis deviated from the outer cylinder shell axis along $x$-axis. (b) Schematic of conventional EBL overlay process. I: Alignment marks process on resist. II: Material deposition and lift-off process. III: Fabricated alignment marks. IV: Subsequent EBL overlay process with the pre-defined alignment marks. Since we have to alignment marks need to be found using electron beam scanning, the alignment marks area uncovered by resists. V: Material deposition for the second layer. VI: Fabricated silica cylinders on the substrate with the pre-defined alignment marks. VII: The third EBL overlay process with silica cylinders and alignment marks. VIII: Material deposition for the third layer. IX: Fabricated non-coaxial core-shell cylinder nanostructure arrays.

The non-coaxial core-shell cylinder nanostructure arrays can be fabricated by electron beam lithography (EBL) overlay [46]. The fabrication process is shown in Fig. 1(b). The first and most important step is making alignment marks (Generally, metals with large atomic numbers such as gold or platinum are used for alignment marks to improve the signal-to-noise ratio) on silica substrate using EBL. The detail process are shown in I-III of Fig. 1(b). Alignment marks can ensure the alignment between layers in process of EBL overlay. Secondly, EBL is also used to fabricate silica cylinders on the substrate with the pre-defined alignment marks as shown in IV-VI of Fig. 1(b). Finally, the silicon cylinder shells are fabricated on the silica cylinders using EBL, which are shown invii-IX of Fig. 1(b).

## 3. Results and discussions

BIC can be transformed into quasi-BIC by symmetry breaking of a unit cell. The symmetry of the core-shell cylinder nanostructure can be controlled by the offset $d$. Figure 2(a) shows the transmission spectra of silicon non-coaxial core-shell cylinder array with different offsets. For $d = 0$ nm (i.e. symmetric structure), there's only one broad spectrum. Once the axis of the inner cylinder core shifts an offset from the axis of the outer cylinder-shell, a sharp spectral resonance

Optics EXPRESS

having the Fano form appears in the transmission spectra, as shown in Fig. 2(a). We plotted the magnetic field, electric field and displacement current distributions of the sharp resonance when $d = 10$ nm in Fig. 2(b). The displacement currents are distributed in closed loops on the surface of the core-shell cylinder along its meridians, such a distribution induces a magnetic vortex with head-to-tail configuration encircling the axis of the cylinder, which is a typical TD resonance mode. The conceptual representation of the TD resonance is visually displayed for a clearer view in Fig. 2(c). Yellow arrows represent the displacement currents, green arrows represent the magnetic dipole (MD) moment ($\vec{M}$) and red arrow shows the TD moment ($\vec{T}$).

As the offset $d$ decreases, the line-width of narrow transmission peak becomes narrower and narrower. When $d = 0$ nm, the narrow peak vanishes. The resonance peak blue shifts from 793.64 to 790.92 nm when $d$ decreases from 30 nm to 5nm. And the wavelength of the resonance peak keeps almost unchanged when $d$ is less than 5 nm. These phenomena indicate that TD resonance is governed by BIC mode. In order to further prove that there is a BIC mode when $d = 0$, we analyzed the resonance mode using Mode Analysis model in COMSOL. The $Q$-factor of resonant mode can reach up to $1.56\times10^9$, which is limited in the calculation by mesh size and tends to infinity for infinitely small mesh size. The $Q$-factor versus the offset $d$ is plotted by the black line in Fig. 2(d). As $d$ decreases from 30 to 1 nm, the $Q$-factor increases exponentially from 213 to $1.73\times10^5$, and increases sharply to $1.56\times10^9$ when $d$ decreases to 0 nm. The variation trend of $Q$ value also conforms to the characteristics of BIC mode [22]. The magnetic field in $x$-$y$ plane and electric field in $y$-$z$ plane of the BIC mode are plotted in the insets in Fig. 2(d). It can be seen that the electric field and magnetic field are similar to that of TD resonance of nanostructure with $d$= 10 nm.

The TD resonance induces the electric field not only to concentrate in the inner cylinder core but also to distribute at the surface of outer cylinder-shell, as shown in Fig. 2(b). The electric field at the surface is very beneficial for chemical biosensing. However, only when BIC transfers to quasi-BIC, it can be applied to chemical biosensors, because BIC cannot be observed in transmission spectrum. We plotted the maximum electric field intensity of the core-shell cylinder with different $d$ by the red line in Fig. 2(d). It can be seen that electric field increases as $d$ decreasing, it can reach up to 367 when the offset $d$ decreases to 1 nm. Even when $d = 10$ nm, which can be fabricated in experiment [47,48], the $Q$-factor and the electric field enhancement can reach to $1.776\times10^3$ and [51–53], respectively. Such high $Q$-factor and strong field distributed on the surface of outer cylinder-shell are significant advantages in sensing application because they can effectively interact with chemobiological analytes.

Multipole decomposition in the Cartesian coordinate is performed to quantitatively identify the TD resonance in our proposed non-coaxial core-shell cylinder structure [49]. The electric dipole ($\vec{P}$), magnetic dipole ($\vec{M}$), toroidal dipole ($\vec{T}$), electric quadrupole ($\vec{Q}_e$) and magnetic quadrupole ($\vec{Q}_m$) are taken into consideration because these five multipoles are usually strongest. The scattered powers of these multipole moments are calculated from:

$$I_p = \frac{2\omega^4}{3c^3}|\vec{P}|^2 \tag{1}$$

$$I_M = \frac{2\omega^4}{3c^3}|\vec{M}|^2 \tag{2}$$

$$I_T = \frac{2\omega^6}{3c^5}|\vec{T}|^2 \tag{3}$$

$$I_{Q_e} = \frac{\omega^6}{5c^5}\sum|\vec{Q}^{(e)}_{\alpha\beta}|^2 \tag{4}$$

$$I_{Q_m} = \frac{\omega^6}{40c^5}\sum|\vec{Q}^{(m)}_{\alpha\beta}|^2 \tag{5}$$

Optics EXPRESS

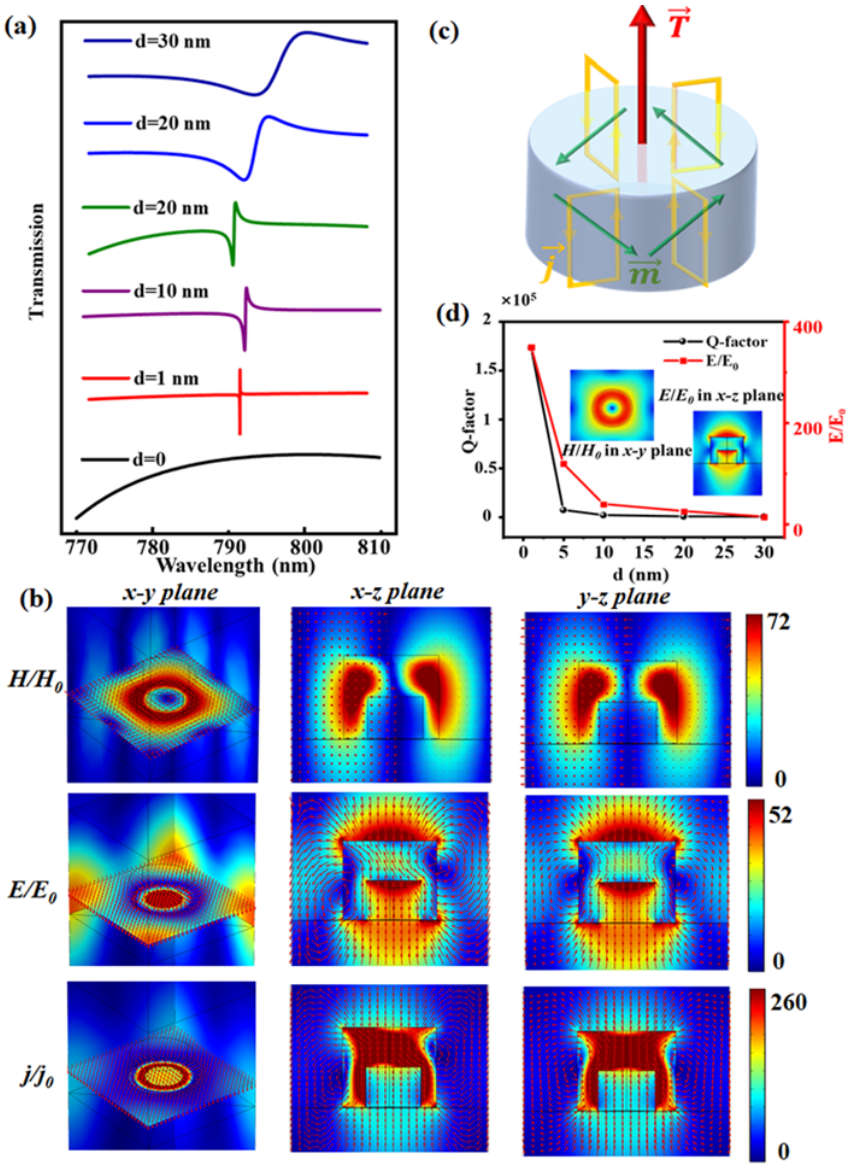


**Fig. 2.** (a) Transmission spectra of silicon non-coaxial core-shell cylinder array with different offset $d$, other structural parameters are $R_1 = 120$ nm, $R_2 = 70$ nm $h_1 = 300$ nm and $h_2 = 100$nm. (b) Distribution of magnetic field enhancement, electric field enhancement, and displacement currents at the TD resonances in the $x$-$y$ (including $x$-$z$, $y$-$z$ planes at the boundary of the compute domain), $x$-$z$ and $y$-$z$ planes (arrows represent the directions of them). (c) The conceptual representation of the TD resonance. (d) The maximum electric field enhancement and $Q$-factors as a function of $d$, other structural parameters are the same as in (a).

Optics EXPRESS

$$\vec{P} = \frac{1}{i\omega}\int \vec{j}\, d^3r \tag{6}$$

$$\vec{M} = \frac{1}{2c}\int (\vec{r}\times\vec{j})d^3r \tag{7}$$

$$\vec{T} = \frac{1}{10c}\int [(\vec{r}\cdot\vec{j})\vec{r} - 2r^2 j]d^3r \tag{8}$$

$$Q^{(e)}_{\alpha\beta} = \frac{1}{2i\omega}\int \left[r_\alpha j_\beta + r_\beta j_\alpha - \frac{2}{3}(\vec{r}\times\vec{j})\delta_{\alpha,\beta}\right]d^3r \tag{9}$$

$$Q^{(m)}_{\alpha\beta} = \frac{1}{3c}\int [(\vec{r}\times\vec{j})_\alpha r_\beta + [(\vec{r}\times\vec{j})_\beta r_\alpha]]d^3r \tag{10}$$

where $\vec{j}$, $c$ and $\omega$ are the displacement current density, the speed and angular frequency of incident light, and $\alpha, \beta = x, y, z$. The decomposition results are shown in Fig. 3. It is clear that the strongest contribution to the resonance is the TD resonance. The secondary contribution to the resonance is magnetic quadrupole. Because the magnetic quadrupole and the toroidal dipole are induced by a pair of counter oriented magnetic dipoles, they are often accompanied by each other. The electric quadrupole also contributes the resonance response. However, the magnetic dipole and electric dipole are strongly suppressed. The above results also demonstrated that the sharp resonance is a TD resonance.

We studied the dependence of the transmission spectra on $R_1$, $R_2$, $h_1$ and $h_2$ in Fig. 4. The offset $d$ of the asymmetric parameter is set as 10 nm. Except for the variable parameters, the other structural parameters are the same as those of the structure used in the Fig. 2(a). From Fig. 4(a-d), we can see that the TD resonance red shifts with the increase of $R_1$ and $h_1$, and with the decrease of $R_2$ and $h_2$. Because when $R_1$ and $h_1$ increase, and $R_2$ and $h_2$ decrease, the effective volume of the outer cylinder shell cavity will increase, which supports the mode with longer resonance wavelength. Figure 4(e-h) show the $Q$-factor and the maximum electric field enhancement of the TD resonance peaks in Fig. 4(a-d), respectively. Here, the $Q$-factors are calculated by $Q = \lambda/\Delta\lambda$, $\lambda$ is the wavelength of the resonance mode, $\Delta\lambda$ is the line-width of the resonance peak, which is almost the same as $Q$ value analyzed by Mode Analysis mode. The $Q$-factor increases from 150.8 to 2348 and the maximum electric field enhancement increases from 19.6 to 66.9 when $R_1$ increases from 100 to 130 nm. Because the asymmetry of nanostructure decrease with the increase of $R_1$ [50]. However, when $R_1$ increases to 140 nm, the $Q$-factor decreases to 1878.4, which caused by the weak coupling (this can be seen from that the narrow peak appears at the edge of the wide spectrum). When $R_2$ decreases, the asymmetry of nanostructure also decreases. The $Q$-factor can increase from 746.1 to 3843.1, and the maximum electric field enhancement can increase from 28.4 to 107.3 when $R_2$ decreases from 90 to 50 nm. However, when the height of outer cylinder shell and inner cylinder core change, although the asymmetry remains unchanged, the $Q$-factor and the electric field also change. When $h_1$ increases from 150 to 300 nm, the $Q$-factor increases from 1163.4 to 3334.5 and the maximum electric field enhancement can increase from 44.3 to 117.4. It needs to be explained that the $Q$-factor increases as $h_1$ decreases from 150 to 130 nm, which is caused by the effect of grating diffraction. When $h_2$ decreases from 200 to 80 nm, the $Q$-factor increases from 827.24 to 2587.7 and the maximum electric field enhancement can increase from 19.6 to 80.7. Because with the increase of $h_1$ and the decrease of $h_2$, the TD resonance is increasingly localized within the outer cylinder shell cavity (as shown in the insets in Fig. 4(g)), which results in a smaller radiation loss.

To demonstrate the sensing performance of the TD resonance supported by the proposed all-dielectric core-shell cylinder nanostructure, we calculated the detection sensitivity $S$ and $FOM$ of the arrays with different parameters in Fig. 5. $S$ is calculated by the shift in the resonance wavelength per refractive-index-unit change of water. $FOM$ is given by $FOM = S \cdot Q/\lambda$, where, $\lambda$

Optics EXPRESS

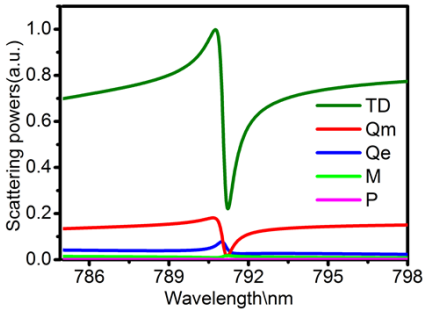


**Fig. 3.** The normalized scattering powers of five strongest multipoles in non-coaxial core-shell cylinder structure with $d$= 10 nm, $R_1 = 120$ nm, $R_2$ =70 nm $h_1 = 300$ nm and $h_2 = 100$nm.

is the wavelength of the resonance mode. We assume that the refractive index of the water layer changes varies from 1.33 to1.37 due to the entry of chemical biomolecules, which will induce the resonance wavelength to shift. When $d$ decreases from 30 to 1 nm, the sensitivity only increases from 273 to 284. While the *FOM* can increase from 167 to $4.04 \times 10^4$, because the $Q$-factor can increase to $1.13 \times 10^5$ when $d = 1$ nm. As $R_1$ increases from 100 to 140 nm, the sensitivity can increase from 250 to 280, the *FOM* can increase up to 832.3. When $R_2$ decreases from 90 to 50 nm, the sensitivity can increase from 240 to 292.2, the *FOM* can increase up to 1380. When $h_1$ increases from 130 to 300 nm, the sensitivity can increase from 60 to 342, the *FOM* can increase up to 1295. When $h_2$ decreases from 80 to 180 nm, the sensitivity can increase from 242 to 286, the *FOM* can increase up to 903. On the basis of these data, it can be seen that the sensitivity is greatly affected by the radius and the height of outer cylinder shell and inner cylinder core, but less affected by the offset $d$. With the increase of $R_1$ and $h_1$ and the decrease of $R_2$ and $h_2$, the effective volume of the outer cylinder shell cavity increases and the relative electric field intensity on its surface will become larger. However, when the offset $d$ changes, the effective volume of the outer cylinder shell cavity basically remains unchanged. A comparison of the sensitivity and *FOM* of our proposed nanostructure to the previously published sensors is shown in Table 1. It's obvious that our proposed nanostructure has high sensitivity and *FOM*. Although the sensitivity of our proposed nanostructure is lower than that of the suspended asymmetric dielectric gratings [43], which is due to the distribution of electric field at the upper and lower surfaces of the suspended structure. Therefore, electromagnetic fields distribute on the surface region of the nanostructure is very important to improve the performance of the sensor.

For biosensing, the surface of metasurface is typically functionalized. Surface sensitivity is also very important in biosensing [54]. We studied the surface sensitivity of nanosensor based on our proposed nanostructure with $d = 10$ nm, $R_1 = 120$ nm, $R_2 = 70$ nm, $h_1 = 200$ nm and$h_2 = 100$ nm. We introduced a homogeneous 10 nm biofilm of index $n_c$ on top of the metasurface. The biofilm mimics a biological perturbation adsorbed on the metasurface. When $n_c$ changes from 1.33 to 1.55, the resonance peak red shifts from 791 to 794.1 nm, as shown in Fig. 6. The surface sensitivity can reach up to 14.1 nm/RIU, which is calculated by the shift in the resonance wavelength per refractive-index-unit change of $n_c$.

Considering the low the extinction coefficient of Si material in the near-infrared region, we didn't consider the imaginary part of refractive index in the transmission spectra calculated above. Figure 7(a) shows the transmission spectrum of nanostructure when the imaginary part of the refractive index ($k$= 0.0071) of silicon is considered [55]. The geometric parameters are $d = 10$ nm, $R_1 = 120$ nm, $R_2 = 70$ nm, $h_1 = 200$ nm and $h_2 = 100$ nm. The resonance wavelength of the quasi-BIC remains unchanged. However, the line-width increases to 1.1 nm, and the $Q$-factor

Optics EXPRESS

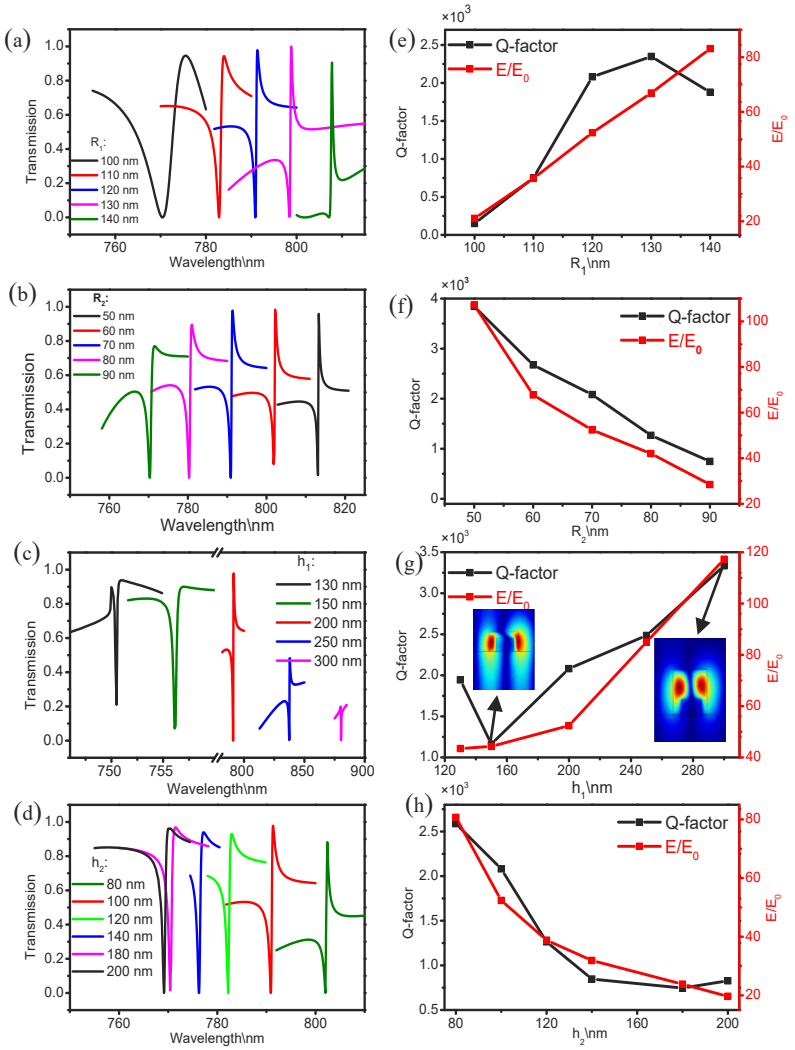


**Fig. 4.** (a-d) Transmission spectra of the all-dielectric non-coaxial core-shell cylinder array with different $R_1$, $R_2$, $h_1$ and $h_2$, the other structural parameters are the same as those of the structures used in the Fig. 2(a) except for the variable parameters. (e-h) The maximum electric field enhancement and $Q$-factors as a function of $R_1$, $R_2$, $h_1$ and $h_2$, other structural parameters are the same as in (a-d). Insets in (g) show the magnetic field distribution in $x$-$z$ plane when $h_1 = 130$ nm and $h_1 = 300$ nm.

Optics EXPRESS

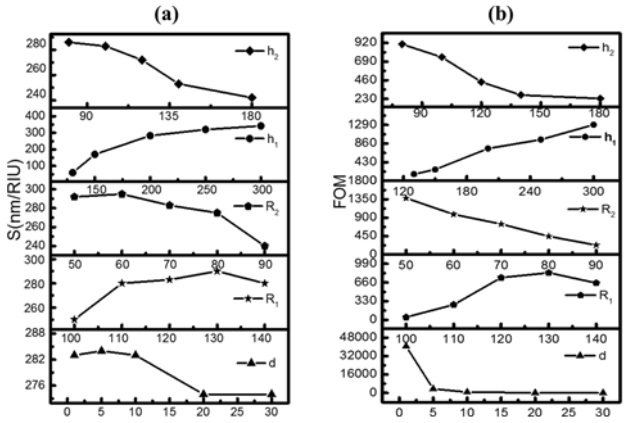


**Fig. 5.** Sensitivities (a) and *FOM* (b) of all-dielectric non-coaxial core-shell cylinder array with different $d$, $R_1$, $R_2$, $h_1$ and $h_2$, the other structural parameters are the same as those of the structure used in the Fig. 2(a) except for the variable parameters.

**Table 1. Comparison of the sensitivity *S* and *FOM* of our proposed structure with previously published sensors**

| Reference | resonance mode and material | | Wavelength (nm) | Sensitivity (nm/RIU) | FOM |
|---|---|---|---|---|---|
| [26] | TD | Si | 950-1250 | 100 | 260 |
| [39] | BIC | $TiO_2$ | 850-880 | 80.6 | 80.6 |
| [40] | BIC | Si | 720-820 | 263 | -- |
| [43] | BIC | Si | 650-775 | 217 | -- |
| [44] | BIC | Si | 1500-1760 | 1506 | 5000 |
| [52] | Hybrid mode | Al+Si | 1232-1344 | 779.4 | -- |
| [53] | Fano | Si | 1100-1450 | 400 | 3074 |
| [54] | BIC | $Si_3N_4$ | 770-790 | 178 | 445 |
| Our work | TD-BIC | Si | 750-880 | 342 | 1295 |

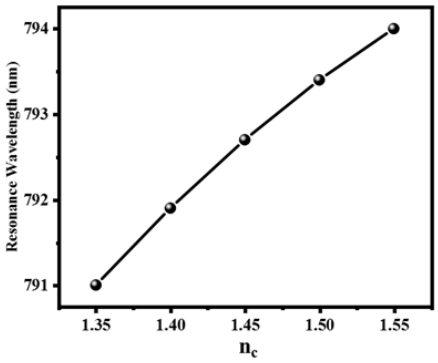


**Fig. 6.** The resonance wavelength of the TD mode as a function of $n_c$. The structure parameters are set as $d = 10$ nm, $R_1 = 120$ nm, $R_2 = 70$ nm, $h_1 = 200$ nm and $h_2 = 100$ nm.

Optics EXPRESS

decreases to 719 because of absorption loss. The biosensing performance is studied in Fig. 7(b). The sensitivities $S$ still can reach up to 285 nm/RIU. However, the *FOM* is down to 259 because of the wider line-width and lower $Q$-factor.

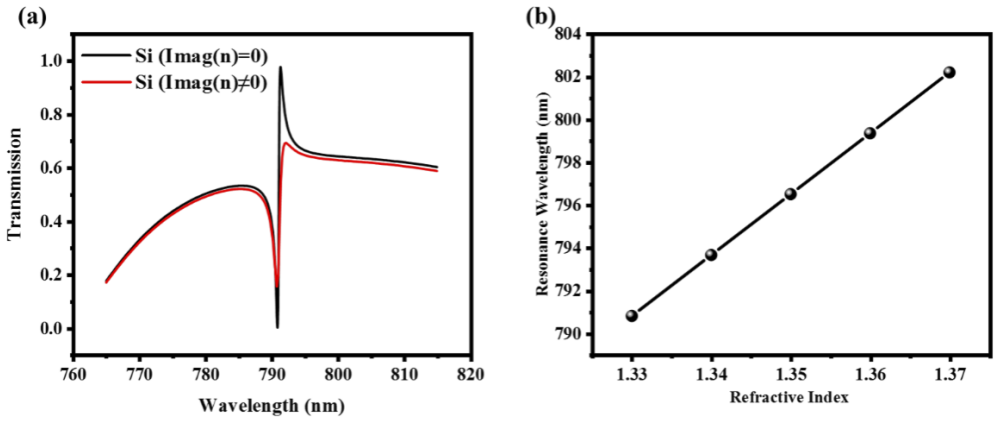


**Fig. 7.** (a) Comparison of transmission spectra of the non-coaxial core-shell cylinder structure with $d = 10$ nm, $R_1 = 120$ nm, $R_2 = 70$ nm, $h_1 = 200$ nm and $h_2 = 100$ nm when the imaginary part of refractive index Imag $(n) \neq 0$ and Imag $(n)$ 0. (b) The resonance wavelength of the TD mode as a function of refractive index of water.

## 4. Conclusions

In summary, we proposed a very sensitive sensor based on the TD resonance governed by BIC in the non-coaxial core-shell cylinder nanostructure in theory. The TD resonance is excited by symmetry-breaking of the nanostructure and has the characteristics of quasi-BIC. It not only has very high $Q$-factor, but also the electric field can distribute at the surface of outer cylinder shell, which are very conducive to improving the performance of the sensor. To evaluate the sensing performance of the proposed structure, the bulk sensitivity and the *FOM* for the bulk sensitivity is predicated as 342 nm/RIU and 1295. Moreover, the toroidal dipole of our proposed nanostructure is excited in an individual dielectric nanostructure under plane wave illumination. Unlike reference [56–58], the excitation of TD resonance in an individual dielectric nanostructure requires special light irradiation. We believe that the proposed nanostructure is of great significance to the research of TD resonance and the development of ultrasensitive sensor.

**Funding.** National Natural Science Foundation of China (91950106, 12174228, 11504209, 11674199); Natural Science Foundation of Shandong Province (ZR2019MA024).

**Disclosures.** The authors declare no conflicts of interest.

**Data availability.** Date underlying the results presented in this paper are not publicly available at this time but may be obtained from the authors upon reasonable request.

## References

1. J. N. Anker, W. P. Hall, O. Lyandres, N. C. Shah, J. Zhao, and R. P. Van Duyne, "Biosensing with plasmonic nanosensors," Nat. Mater. **7**(6), 442–453 (2008).
2. P. Zijlstra, P. M. R. Paulo, and M. Orrit, "Optical detection of single non-absorbing molecules using the surface plasmon resonance of a gold nanorod," Nat. Nanotechnol. **7**(6), 379–382 (2012).
3. F. Monticone and A. Alu, "Metamaterial, plasmonic and nanophotonic devices," Rep. Prog. Phys. **80**(3), 036401 (2017).
4. J. Wang and J. Du, "Plasmonic and Dielectric Metasurfaces: Design, Fabrication and Applications," Appl. Sci. **6**(9), 239 (2016).
5. M. L. Tseng, X. Fang, V. Savinov, P. C. Wu, J. Y. Ou, N. I. Zheludev, and D. P. Tsai, "Coherent selection of invisible high-order electromagnetic excitations," Sci. Rep. **7**(1), 44488 (2017).

Optics EXPRESS


6. Y. M. Yang, I. I. Kravchenko, D. P. Briggs, and J. Valentine, "All-dielectric metasurface analogue of electromagnetically induced transparency," Nat. Commun. **5**(1), 5753 (2014).
7. S. V. Li, D. G. Baranov, A. E. Krasnok, and P. A. Belov, "All-dielectric nanoantennas for unidirectional excitation of electromagnetic guided modes," Appl. Phys. Lett. **107**(17), 171101 (2015).
8. R. Regmi, J. Berthelot, P. M. Winkler, M. Mivelle, J. Proust, F. Bedu, I. Ozerov, T. Begou, J. Lumeau, H. Rigneault, M. F. Garcia-Parajo, S. Bidault, J. Wenger, and N. Bonod, "All-Dielectric Silicon Nanogap Antennas To Enhance the Fluorescence of Single Molecules," Nano Lett. **16**(8), 5143–5151 (2016).
9. A. Tittl, A. Leitis, M. K. Liu, F. Yesilkoy, D. Y. Choi, D. N. Neshev, Y. S. Kivshar, and H. Altug, "Imaging-based molecular barcoding with pixelated dielectric metasurfaces," Science **360**(6393), 1105–1109 (2018).
10. M. Semmlinger, M. Zhang, M. L. Tseng, T. T. Huang, J. Yang, D. P. Tsai, P. Nordlander, and N. J. Halas, "Generating Third Harmonic Vacuum Ultraviolet Light with a $TiO_2$ Metasurface," Nano Lett. **19**(12), 8972–8978 (2019).
11. N. Bontempi, L. Carletti, C. De Angelis, and I. Alessandri, "Plasmon-free SERS detection of environmental $CO_2$ on $TiO_2$ surfaces," Nanoscale **8**(6), 3226–3231 (2016).
12. A. I. Kuznetsov, A. E. Miroshnichenko, M. L. Brongersma, Y. S. Kivshar, and B. Luk'yanchuk, "Optically resonant dielectric nanostructures," Science **354**(6314), 846–854 (2016).
13. N. Bontempi, K. E. Chong, H. W. Orton, I. Staude, D. Y. Choi, I. Alessandri, Y. S. Kivshar, and D. N. Neshev, "Highly sensitive biosensors based on all-dielectric nanoresonators," Nanoscale **9**(15), 4972–4980 (2017).
14. O. Yavas, M. Svedendahl, P. Dobosz, V. Sanz, and R. Quidant, "On-a-chip Biosensing Based on All-Dielectric Nanoresonators," Nano Lett. **17**(7), 4421–4426 (2017).
15. M. L. Tseng, A. Jahani, A. Leitis, and H. Altug, "Dielectric Metasurfaces Enabling Advanced Optical Biosensors," ACS Photonics **8**(1), 47–60 (2021).
16. N. Papasimakis, V. A. Fedotov, V. Savinov, T. A. Raybould, and N. I. Zheludev, "Electromagnetic toroidal excitations in matterand free space," Nat. Mater. **15**(3), 263–271 (2016).
17. T. Kaelberer, V. A. Fedotov, N. Papasimakis, D. P. Tsai, and N. I. Zheludev, "Toroidal Dipolar Response in a Metamaterial," Science **330**(6010), 1510–1512 (2010).
18. L. Y. Guo, M. H. Li, X. J. Huang, and H. L. Yang, "Electric toroidal metamaterial for resonant transparency and circular cross-polarization conversion," Appl. Phys. Lett. **105**(3), 033507 (2014).
19. C. Chen, K. Kaj, Y. Huang, X. Zhao, R. D. Averitt, and X. Zhang, "Tunable Toroidal Response in a Reconfigurable Terahertz Metamaterial," Adv. Opt. Mater. **9**(22), 2101215 (2021).
20. V. A. Fedotov, A. V. Rogacheva, V. Savinov, D. P. Tsai, and N. I. Zheludev, "Resonant Transparency and Non-Trivial Non-Radiating Excitations in Toroidal Metamaterials," Sci. Rep. **3**(1), 2967 (2013).
21. V. R. Tuz, V. V. Khardikov, and Y. S. Kivshar, "All-Dielectric Resonant Metasurfaces with a Strong Toroidal Response," ACS Photonics **5**(5), 1871–1876 (2018).
22. V. R. Tuz, V. Dmitriev, and A. B. Evlyukhin, "Antitoroidic and Toroidic Orders in All-Dielectric Metasurfaces for Optical Near-Field Manipulation," ACS Appl. Nano Mater. **3**(11), 11315–11325 (2020).
23. A. Sayanskiy, M. Danaeifar, P. Kapitanova, and A. E. Miroshnichenko, "All-Dielectric Metalattice with Enhanced Toroidal Dipole," Adv. Opt. Mater. **6**(19), 1800302 (2018).
24. F. Yan, Q. Li, Z. Wang, H. Tian, and L. Li, "Extremely high Q-factor terahertz metasurface using reconstructive coherent mode resonance," Opt. Express **29**(5), 7015–7023 (2021).
25. Y. L. Wang, Z. H. Han, Y. Du, and J. Qin, "Ultrasensitive terahertz sensing with high-Q toroidal dipole resonance governed by bound states in the continuum in all-dielectric metasurface," Nanophotonics **10**(4), 1295–1307 (2021).
26. W. Wang, J. Qi, and B. Li, "Gap-enhanced toroidal dipole and magnetic Fano resonances with polarization independence in all-dielectric metamaterials for sensing," J. Nanophotonics **14**(4), 046006 (2020).
27. A. A. Basharin, M. Kafesaki, E. N. Economou, C. M. Soukoulis, V. A. Fedotov, V. Savinov, and N. I. Zhelude, "Dielectric metamaterials with toroidal dipolar response," Phys. Rev. X **5**(1), 011036 (2015).
28. K. Koshelev, S. Lepeshov, M. K. Liu, A. Bogdanov, and Y. Kivshar, "Asymmetric Metasurfaces with High-Q Resonances Governed by Bound States in the Continuum," Phys. Rev. Lett. **121**(19), 193903 (2018).
29. H. Friedrich and D. Wintgen, "Interfering resonances and bound states in the continuum," Phys. Rev. A **32**(6), 3231–3242 (1985).
30. S. Han, L. Q. Cong, Y. K. Srivastava, B. Qiang, M. V. Rybin, A. Kumar, R. Jain, W. X. Lim, V. C. Achanta, S. S. Prabhu, Q. J. Wang, Y. S. Kivshar, and R. Singh, "All-Dielectric Active Terahertz Photonics Driven by Bound States in the Continuum," Adv. Mater. **31**(37), 1901921 (2019).
31. C. W. Hsu, B. Zhen, A. D. Stone, J. D. Joannopoulos, and M. Soljacic, "Bound states in the continuum," Nat. Rev. Mater. **1**(9), 16048 (2016).
32. T. Y. Ning, X. Li, Y. Zhao, L. Y. Yin, Y. Y. Huo, L. N. Zhao, and Q. Y. Yue, "Giant enhancement of harmonic generation in all-dielectric resonant waveguide gratings of quasi-bound states in the continuum," Opt. Express **28**(23), 34024–34034 (2020).
33. K. Koshelev, G. Favraud, A. Bogdanov, Y. Kivshar, and A. Fratalocchi, "Nonradiating photonics with resonant dielectric nanostructures," Nanophotonics **8**(5), 725–745 (2019).
34. W. Bi, X. Zhang, M. Yan, L. Zhao, T. Ning, and Y. Huo, "Low-threshold and controllable nanolaser based on quasi-BIC supported by all-dielectric eccentric nanoring structure," Opt. Express **29**(8), 12634–12643 (2021).
35. C. Huang, C. Zhang, S. M. Xiao, Y. H. Wang, Y. B. Fan, Y. L. Liu, N. Zhang, G. Y. Qu, H. J. Ji, J. C. Han, L. Ge, Y. Kivshar, and Q. H. Song, "Ultrafast control of vortex microlasers," Science **367**(6481), 1018–1021 (2020).

Optics EXPRESS


36. X. Chen and W. H. Fan, "Ultrahigh-Q toroidal dipole resonance in all-dielectric metamaterials for terahertz sensing," Opt. Lett. **44**(23), 5876–5879 (2019).
37. S. Romano, A. Lamberti, M. Masullo, E. Penzo, S. Cabrini, I. Rendina, and V. Mocella, "Optical Biosensors Based on Photonic Crystals Supporting Bound States in the Continuum," Materials **11**(4), 526 (2018).
38. Y. Chen, C. Zhao, Y. Z. Zhang, and C. W. Qiu, "Integrated Molar Chiral Sensing Based on High-Q Metasurface," Nano Lett. **20**(12), 8696–8703 (2020).
39. F. Yesilkoy, E. R. Arvelo, Y. Jahani, M. K. Liu, A. Tittl, V. Cevher, Y. Kivshar, and H. Altug, "Ultrasensitive hyperspectral imaging and biodetection enabled by dielectric metasurfaces," Nat. Photonics **13**(6), 390–396 (2019).
40. E. Di Fabrizio, S. Schlucker, J. Wenger, R. Regmi, H. Rigneault, G. Calafiore, M. West, S. Cabrini, M. Fleischer, N. F. van Hulst, M. F. Garcia-Parajo, A. Pucci, D. Cojoc, C. A. E. Hauser, and M. Ni, "Roadmap on biosensing and photonics with advanced nano-optical methods," J. Opt. **18**(6), 063003 (2016).
41. S. Romano, M. Mangini, E. Penzo, S. Cabrini, A. C. D. Luca, I. Rendina, V. Mocella, and G. Zito, "Ultrasensitive Surface Refractive Index Imaging Based on Quasi-Bound States in the Continuum," ACS Nano **14**(11), 15417–15427 (2020).
42. J. Wang, J. Kühne, T. Karamanos, C. Rockstuhl, S. A. Maier, and A. Tittl, "All-Dielectric Crescent Metasurface Sensor Driven by Bound States in the Continuum," Adv. Funct. Mater. **31**(46), 2104652 (2021).
43. C. Liu, Y. Bai, J. Zhou, J. Chen, and L. Qiao, "Refractive index sensing by asymmetric dielectric gratings with both bound states in the continuum and guided mode resonances," Opt. Express **29**(26), 42978–42988 (2021).
44. U. Zywietz, A. B. Evlyukhin, C. Reinhardt, and B. N. Chichkov, "Laser printing of silicon nanoparticles with resonant optical electric and magnetic responses," Nat. Commun. **5**(1), 3402 (2014).
45. S. Y. Li, C. B. Zhou, T. T. Liu, and S. Y. Xiao, "Symmetry-protected bound states in the continuum supported by all-dielectric metasurfaces," Phys. Rev. A **100**(6), 063803 (2019).
46. G. Yoon, I. Kim, S. So, J. Mun, M. Kim, and J. Rho, "Fabrication of three-dimensionalsuspended, interlayered andhierarchical nanostructures by accuracy-improved electron beam lithography overlay," Sci. Rep. **7**(1), 6668 (2017).
47. L. Zhao, Y. Wei, and T. Ye, "Analysis of multi-e-beam lithography for cutting layers at 7-nm node," J. Micro/Nanolith. MEMS MOEMS **15**(4), 043501 (2016).
48. B. E. Maile, W. Henschel, H. Kurz, B. Rienks, R. Polman, and P. Kaars, "Sub-10 nm Linewidth and Overlay PerformanceAchieved with a Fine-Tuned EBPG-5000 TFEElectron Beam Lithography System," Jpn. J. Appl. Phys. **39**(Part 1, No. 12B), 6836–6842 (2000).
49. C. Zhou, S. Li, Y. Wang, and M. Zhan, "Multiple toroidal dipole Fano resonances of asymmetric dielectric nanohole arrays," Phys. Rev. B **100**(19), 195306 (2019).
50. X. Wang, J. Duan, W. Chen, C. Zhou, T. Liu, and S. Xiao, "Controlling light absorption of graphene at critical coupling through magnetic dipole quasi-bound states in the continuum resonance," Phys. Rev. B **102**(15), 155432 (2020).
51. D. Ray, T. V. Raziman, C. Santschi, D. Etezadi, H. Altug, and O. J. F. Martin, "Hybrid Metal-Dielectric Metasurfaces for Refractive Index Sensing," Nano Lett. **20**(12), 8752–8759 (2020).
52. W. Su, Z. Geng, J. Qi, and H. Wu, "Multi-Fano Resonances In Graphene Coated All-dielectric Metasurface For Refractive Index Sensing With High Figure Of Merits," IEEE J. Sel. Top. Quantum Electron. **27**(1), 1–6 (2021).
53. S. Romano, G. Zito, S. Torino, G. Calafiore, E. Penzo, G. Coppola, S. Cabrini, I. Rendina, and V. Mocella, "Label-free sensing of ultralow-weight molecules with all-dielectric metasurfaces supporting bound states in the continuum," Photonics Res. **6**(7), 726–733 (2018).
54. G. Zito, G. Sanità, B. G. Alulema, S. N. L. Yépez, V. Lanzio, F. Riminucci, S. Cabrini, M. Moccia, C. Avitabile, A. Lamberti, and V. Mocella, "Label-free DNA biosensing by topological light confinement," Nanophotonics **10**(17), 4279–4287 (2021).
55. D. E. Aspnes and A. A. Studna, "Dielectric functions and optical parameters of Si, Ge, GaP, GaAs, GaSb, InP, InAs, and InSb from 1.5 to 6.0 eV," Phys. Rev. B **27**(2), 985–1009 (1983).
56. R. M. Saadabad, M. Cai, F. Deng, L. Xu, and A. E. Miroshnichenko, "Structured light excitation of toroidal dipoles in dielectric nanodisks," Phys. Rev. B **104**(16), 165402 (2021).
57. J. A. Parker, H. Sugimoto, B. Coe, D. Eggena, M. Fujii, N. F. Scherer, S. K. Gray, and U. Manna, "Excitation of Nonradiating Anapoles in Dielectric Nanospheres," Phys. Rev. Lett. **124**(9), 097402 (2020).
58. J. Xu, H. Fan, Q. Dai, H. Liu, and S. Lan, "Toroidal dipole response in the individual silicon hollow cylinder under radially polarized beam excitation," J. Phys. D: Appl. Phys. **54**(21), 215102 (2021).